Submitted to the 29th International Conference on High-Energy Physics ICHEP98,
Vancouver, Canada, July 1998

DESY 98-063 ISSN 0418-9833
May 1998

Observation of Events with an Isolated High Energy Lepton and Missing Transverse Momentum at HERA

H1 Collaboration

Abstract

A search for events with an imbalance in transverse momentum and with isolated high energy leptons has been carried out at the positron-proton collider HERA. One event with an e^- and five events with a $\mu^\pm$ are found together with evidence for undetected particles carrying transverse momentum. Within the Standard Model the dominant origin of events with this kind of topology is the production of W bosons with subsequent leptonic decay. Three of the six events are within measurement errors found in a region of phase space likely to be populated by this process, while the remaining events show kinematic properties which are atypical of all Standard Model processes considered.

Abstract: 578
Parallel sessions: 1,10
Plenary sessions: 1,12

C. Adloff[34], M. Anderson[22], V. Andreev[25], B. Andrieu[28], V. Arkadov[35], C. Arndt[11], I. Ayyaz[29], A. Babaev[24], J. Bähr[35], J. Bán[17], P. Baranov[25], E. Barrelet[29], R. Barschke[11], W. Bartel[11], U. Bassler[29], P. Bate[22], M. Beck[13], A. Beglarian[11,40], O. Behnke[11], H.-J. Behrend[11], C. Beier[15], A. Belousov[25], Ch. Berger[1], G. Bernardi[29], G. Bertrand-Coremans[4], P. Biddulph[22], J.C. Bizot[27], V. Boudry[28], A. Braemer[14], W. Braunschweig[1], V. Brisson[27], D.P. Brown[22], W. Brückner[13], P. Bruel[28], D. Bruncko[17], J. Bürger[11], F.W. Büsser[12], A. Buniatian[32], S. Burke[18], G. Buschhorn[26], D. Calvet[23], A.J. Campbell[11], T. Carli[26], E. Chabert[23], M. Charlet[4], D. Clarke[5], B. Clerbaux[4], S. Cocks[19], J.G. Contreras[8], C. Cormack[19], J.A. Coughlan[5], M.-C. Cousinou[23], B.E. Cox[22], G. Cozzika[9], J. Cvach[30], J.B. Dainton[19], W.D. Dau[16], K. Daum[39], M. David[9], M. Davidsson[21], A. De Roeck[11], E.A. De Wolf[4], B. Delcourt[27], C. Diaconu[23], M. Dirkmann[8], P. Dixon[20], W. Dlugosz[7], K.T. Donovan[20], J.D. Dowell[3], A. Droutskoi[24], J. Ebert[34], G. Eckerlin[11], D. Eckstein[35], V. Efremenko[24], S. Egli[37], R. Eichler[36], F. Eisele[14], E. Eisenhandler[20], E. Elsen[11], M. Enzenberger[26], M. Erdmann[14,41,f], A.B. Fahr[12], L. Favart[4], A. Fedotov[24], R. Felst[11], J. Feltesse[9], J. Ferencei[17], F. Ferrarotto[32], M. Fleischer[8], G. Flügge[2], A. Fomenko[25], J. Formánek[31], J.M. Foster[22], G. Franke[11], E. Gabathuler[19], K. Gabathuler[33], F. Gaede[26], J. Garvey[3], J. Gayler[11], M. Gebauer[35], R. Gerhards[11], S. Ghazaryan[11,40], A. Glazov[35], L. Goerlich[6], N. Gogitidze[25], M. Goldberg[29], I. Gorelov[24], C. Grab[36], H. Grässler[2], T. Greenshaw[19], R.K. Griffiths[20], G. Grindhammer[26], C. Gruber[16], T. Hadig[1], D. Haidt[11], L. Hajduk[6], T. Haller[13], M. Hampel[1], V. Haustein[34], W.J. Haynes[5], B. Heinemann[11], G. Heinzelmann[12], R.C.W. Henderson[18], S. Hengstmann[37], H. Henschel[35], R. Heremans[4], I. Herynek[30], K. Hewitt[3], K.H. Hiller[35], C.D. Hilton[22], J. Hladký[30], D. Hoffmann[11], T. Holtom[19], R. Horisberger[33], V.L. Hudgson[3], S. Hurling[11], M. Ibbotson[22], Ç. İşsever[8], H. Itterbeck[1], M. Jacquet[27], M. Jaffre[27], D.M. Jansen[13], L. Jönsson[21], D.P. Johnson[4], H. Jung[21], H.-C. Kaestli[36], M. Kander[11], D. Kant[20], M. Karlsson[21], U. Kathage[16], J. Katzy[11], H.H. Kaufmann[35], O. Kaufmann[14], M. Kausch[11], I.R. Kenyon[3], S. Kermiche[23], C. Keuker[1], C. Kiesling[26], M. Klein[35], C. Kleinwort[11], G. Knies[11], J.H. Köhne[26], H. Kolanoski[38], S.D. Kolya[22], V. Korbel[11], P. Kostka[35], S.K. Kotelnikov[25], T. Krämerkämper[8], M.W. Krasny[29], H. Krehbiel[11], D. Krücker[26], A. Küpper[34], H. Küster[21], M. Kuhlen[26], T. Kurca[35], B. Laforge[9], R. Lahmann[11], M.P.J. Landon[20], W. Lange[35], U. Langenegger[36], A. Lebedev[25], F. Lehner[11], V. Lemaitre[11], S. Levonian[11], M. Lindstroem[21], B. List[11], G. Lobo[27], V. Lubimov[24], D. Lüke[8,11], L. Lytkin[13], N. Magnussen[34], H. Mahlke-Krüger[11], E. Malinovski[25], R. Maracek[17], P. Marage[4], J. Marks[14], R. Marshall[22], G. Martin[12], H.-U. Martyn[1], J. Martyniak[6], S.J. Maxfield[19], S.J. McMahon[19], T.R. McMahon[19], A. Mehta[5], K. Meier[15], P. Merkel[11], F. Metlica[13], A. Meyer[12], A. Meyer[11], H. Meyer[34], J. Meyer[11], P.-O. Meyer[2], A. Migliori[28], S. Mikocki[6], D. Milstead[11], J. Moeck[26], R. Mohr[26], S. Mohrdieck[12], F. Moreau[28], J.V. Morris[5], E. Mroczko[6], D. Müller[37], K. Müller[11], P. Murffi[17], V. Nagovizin[24], B. Naroska[12], Th. Naumann[35], I. Négri[23], P.R. Newman[3], D. Newton[18], H.K. Nguyen[29], T.C. Nicholls[11], F. Niebergall[12], C. Niebuhr[11], Ch. Niedzballa[1], H. Niggli[36], O. Nix[15], G. Nowak[6], T. Nunnemann[13], H. Oberlack[26], J.E. Olsson[11], D. Ozerov[24], P. Palmen[2], E. Panaro[11], A. Panitch[4], C. Pascaud[27], S. Passaggio[36], G.D. Patel[19], H. Pawletta[2], E. Peppel[35], E. Perez[9], J.P. Phillips[19], A. Pieuchot[11], D. Pitzl[36], R. Pöschl[8], G. Pope[7], B. Povh[13], K. Rabbertz[1], P. Reimer[30], B. Reisert[26], H. Rick[11], S. Riess[12], E. Rizvi[11], P. Robmann[37], R. Roosen[4], K. Rosenbauer[1], A. Rostovtsev[24,11], F. Rouse[7], C. Royon[9], S. Rusakov[25], K. Rybicki[6], D.P.C. Sankey[5], P. Schacht[26], J. Scheins[1], S. Schiek[11], S. Schleif[15], P. Schleper[14], D. Schmidt[34], G. Schmidt[11], L. Schoeffel[9], A. Schöning[11], V. Schröder[11], H.-C. Schultz-Coulon[11], B. Schwab[14], F. Sefkow[37], A. Semenov[24], V. Shekelyan[26], I. Sheviakov[25], L.N. Shtarkov[25], G. Siegmon[16], U. Siewert[16], Y. Sirois[28], I.O. Skillicorn[10], T. Sloan[18], P. Smirnov[25], M. Smith[19], V. Solochenko[24], Y. Soloviev[25], A. Specka[28], J. Spiekermann[8], H. Spitzer[12], F. Squinabol[27], P. Steffen[11], R. Steinberg[2], J. Steinhart[12], B. Stella[32], A. Stellberger[15], J. Stiewe[15], U. Straumann[14], W. Struczinski[2], J.P. Sutton[3], M. Swart[15], S. Tapprogge[15], M. Tasevský[31], V. Tchernyshov[24], S. Tchetchelnitski[24], J. Theissen[2], G. Thompson[20], P.D. Thompson[3], N. Tobien[11], R. Todenhagen[13], P. Truöl[37], G. Tsipolitis[36], J. Turnau[6], E. Tzamariudaki[11], S. Udluft[26], A. Usik[25], S. Valkár[31], A. Valkárová[31], C. Vallée[23], P. Van Esch[4], P. Van Mechelen[4], Y. Vazdik[25], G. Villet[9], K. Wacker[8], R. Wallny[14], T. Walter[37], B. Waugh[22], G. Weber[12], M. Weber[15], D. Wegener[8], A. Wegner[26], T. Wengler[14], M. Werner[14], L.R. West[3], S. Wiesand[34], T. Wilksen[11], S. Willard[7], M. Winde[35], G.-G. Winter[11], C. Wittek[12], E. Wittmann[13], M. Wobisch[2], H. Wollatz[11], E. Wünsch[11], J. Zácek[31], J. Zálesák[31], Z. Zhang[27], A. Zhokin[24], P. Zini[29], F. Zomer[27], J. Zsembery[9] and M. zurNedden[37]

[1] I. Physikalisches Institut der RWTH, Aachen, Germany[a]
[2] III. Physikalisches Institut der RWTH, Aachen, Germany[a]
[3] School of Physics and Space Research, University of Birmingham, Birmingham, UK[b]
[4] Inter-University Institute for High Energies ULB-VUB, Brussels; Universitaire Instelling Antwerpen, Wilrijk; Belgium[c]
[5] Rutherford Appleton Laboratory, Chilton, Didcot, UK[b]
[6] Institute for Nuclear Physics, Cracow, Poland[d]
[7] Physics Department and IIRPA, University of California, Davis, California, USA[e]
[8] Institut für Physik, Universität Dortmund, Dortmund, Germany[a]
[9] DSM/DAPNIA, CEA/Saclay, Gif-sur-Yvette, France
[10] Department of Physics and Astronomy, University of Glasgow, Glasgow, UK[b]
[11] DESY, Hamburg, Germany[a]
[12] II. Institut für Experimentalphysik, Universität Hamburg, Hamburg, Germany[a]
[13] Max-Planck-Institut für Kernphysik, Heidelberg, Germany[a]
[14] Physikalisches Institut, Universität Heidelberg, Heidelberg, Germany[a]
[15] Institut für Hochenergiephysik, Universität Heidelberg, Heidelberg, Germany[a]
[16] Institut für experimentelle und angewandte Physik, Universität Kiel, Kiel, Germany[a]
[17] Institute of Experimental Physics, Slovak Academy of Sciences, Kosice, Slovak Republic[f,j]
[18] School of Physics and Chemistry, University of Lancaster, Lancaster, UK[b]
[19] Department of Physics, University of Liverpool, Liverpool, UK[b]
[20] Queen Mary and Westfield College, London, UK[b]
[21] Physics Department, University of Lund, Lund, Sweden[g]
[22] Department of Physics and Astronomy, University of Manchester, Manchester, UK[b]
[23] CPPM, Université d' Aix-Marseille II, IN2P3-CNRS, Marseille, France
[24] Institute for Theoretical and Experimental Physics, Moscow, Russia
[25] Lebedev Physical Institute, Moscow, Russia[f,k]
[26] Max-Planck-Institut für Physik, München, Germany[a]
[27] LAL, Université de Paris-Sud, IN2P3-CNRS, Orsay, France
[28] LPNHE, Ecole Polytechnique, IN2P3-CNRS, Palaiseau, France
[29] LPNHE, Universités Paris VI and VII, IN2P3-CNRS, Paris, France
[30] Institute of Physics, Academy of Sciences of the Czech Republic, Praha, Czech Republic[f,h]
[31] Nuclear Center, Charles University, Praha, Czech Republic[f,h]
[32] INFN Roma 1 and Dipartimento di Fisica, Universita Roma 3, Roma, Italy
[33] Paul Scherrer Institut, Villigen, Switzerland
[34] Fachbereich Physik, Bergische Universität Gesamthochschule Wuppertal, Wuppertal, Germany[a]
[35] DESY, Institut für Hochenergiephysik, Zeuthen, Germany[a]
[36] Institut für Teilchenphysik, ETH, Zürich, Switzerland[i]
[37] Physik-Institut der Universität Zürich, Zürich, Switzerland[i]
[38] Institut für Physik, Humboldt-Universität, Berlin, Germany[a]
[39] Rechenzentrum, Bergische Universität Gesamthochschule Wuppertal, Wuppertal, Germany[a]
[40] Visitor from Yerevan Physics Institute, Armenia
[41] Institut für Experimentelle Kernphysik, Universität Karlsruhe, Karlsruhe, Germany

[a] Supported by the Bundesministerium für Bildung, Wissenschaft, Forschung und Technologie, FRG, under contract numbers 7AC17P, 7AC47P, 7DO55P, 7HH17I, 7HH27P, 7HD17P, 7HD27P, 7KI17I, 6MP17I and 7WT87P
[b] Supported by the UK Particle Physics and Astronomy Research Council, and formerly by the UK Science and Engineering Research Council
[c] Supported by FNRS-NFWO, IISN-IIKW
[d] Partially supported by the Polish State Committee for Scientific Research, grant no. 115/E-343/SPUB/P03/002/97 and grant no. 2P03B 055 13
[e] Supported in part by US DOE grant DE F603 91ER40674

[f] Supported by the Deutsche Forschungsgemeinschaft
[g] Supported by the Swedish Natural Science Research Council
[h] Supported by GA CR grant no. 202/96/0214, GA AV CR grant no. A1010619 and GA UK grant no. 177
[i] Supported by the Swiss National Science Foundation
[j] Supported by VEGA SR grant no. 2/1325/96
[k] Supported by Russian Foundation for Basic Researches grant no. 96-02-00019

1 Introduction

At the HERA collider the study of rare topologies in the final state of electron[1]-proton interactions provides a unique possibility to search for new phenomena. In this paper, a search for events with an imbalance in transverse momentum and isolated high energy leptons is reported. In 1994 the first event with such a signature ($e^+p \rightarrow \mu^+ X$) was observed [1, 2] in the H1 detector. Within the Standard Model (SM), such topologies are expected mainly from the production of W bosons with subsequent leptonic decay. A significant excess of events compared to SM expectations might reflect anomalous electroweak three-boson couplings [3], or production of new particles as expected for example in supersymmetric extensions of the SM [4].

The present analysis is based on positron (27.5 GeV) - proton (820 GeV) collisions recorded by the H1 experiment between 1994 and 1997. The total integrated luminosity is 36.5 ± 1.1 pb^{-1}, an order of magnitude higher than in the earlier studies cited above.

2 Data Analysis

2.1 Experimental Conditions

A detailed description of the H1 detector can be found in [5]. Here we only summarize those properties of components essential for this analysis[2].

A central tracker consisting of drift chambers is used to measure the charged particle trajectories and to determine the interaction vertex. Particle transverse momenta are determined from the curvature of the trajectories in a magnetic field of 1.15 Tesla.

Electromagnetic and hadronic final state particles are absorbed in a highly segmented liquid argon calorimeter [6] covering the polar angular range $4^\circ < \theta < 153^\circ$. The calorimeter is 5 to 8 interaction lengths deep depending on the polar angle of the particle. Electromagnetic shower energies are measured with a precision of $\sigma(E)/E = 12\%/\sqrt{E/\mathrm{GeV}} \oplus 1\%$ and hadronic shower energies with $\sigma(E)/E = 50\%/\sqrt{E/\mathrm{GeV}} \oplus 2\%$ [7] using software-based energy weighting techniques. The absolute energies are known to 3% and 4% respectively. The liquid argon calorimeter is complemented in the backward region by a lead/scintillating-fibre calorimeter[3] [8] covering the range $155^\circ < \theta < 178^\circ$, and by positron and photon taggers located downstream of the interaction point in the positron beam direction.

The calorimeter is surrounded by a superconducting coil and an iron yoke instrumented with streamer tubes. Leakage of hadronic showers outside the calorimeter is measured by the analogue charge sampling of the streamer tubes (Tail Catcher) with a resolution of $\sigma(E)/E = 100\%/\sqrt{E/\mathrm{GeV}}$. Tracks of penetrating charged particles, such as muons, escaping the calorimeter are reconstructed from their hit pattern in the streamer tubes with an efficiency greater than 80%.

The trigger condition for interactions involving high transverse energy is derived from the liquid argon calorimeter signals. The trigger efficiency is greater than 95% for events with a scattered electron which has energy above 10 GeV, and greater than 85% for events with a calorimetric missing transverse momentum which is greater than 25 GeV.

[1] In this paper the term `electron' is used to describe generically electrons or positrons.

[2] The origin of the coordinate system is the nominal ep interaction point. The direction of the incoming proton defines the z-axis for the measurement of polar and azimuthal angles as well as for transverse momenta. It also defines the forward region of the detector. The modulus of a vector $\vec{V}$ is denoted V.

[3] This device was installed in 1995 replacing a lead-scintillator "sandwich" calorimeter.

2.2 Event Selection

The selection procedure uses methods developed in the framework of H1 Charged Current (CC) analyses [9]. A search for an imbalance in transverse momentum with isolated high energy leptons is based on two independent requirements:

- The calorimetric missing transverse momentum, P_T^{calo}, must be greater than 25 GeV.

  P_T^{calo} is defined as the transverse component of the vector sum of all energy deposits recorded in the liquid argon calorimeter and the tail catcher. The cut value of 25 GeV is chosen to minimize contributions from Neutral Current (NC) deep-inelastic scattering (DIS), photoproduction and photon-photon processes, as well as from non-ep background.

- There must be at least one well measured central track with a polar angle greater than $10°$ and a transverse momentum greater than 10 GeV.

  The cut value of 10 GeV is designed to minimize the contribution from semi-leptonic decays of heavy mesons. Tracks fulfilling the above requirements are referred to as *high-P_T tracks* in the following.

Non-ep events due to cosmic muons, halo muons or beam-gas interactions are removed by using a set of topological and timing requirements [9] and by demanding a reconstructed vertex in the ep interaction region. Residual NC events with energy loss in the calorimeter cracks or in the beam-pipe are eliminated by excluding events with an identified scattered positron under the following conditions: either the positron is balanced by the hadronic system in azimuth within $\Delta\phi = 5°$, or the longitudinal momentum balance results in $\delta > 45$ GeV. Here $\delta = \sum E_i(1 - \cos\theta_i)$, where E_i and θ_i denote the energy and polar angle of each detected final state particle. For an event where only longitudinal momentum along the proton direction (proton-remnant region) is undetected, one expects $\delta = 2E_e = 55$ GeV, where E_e is the energy of the incident positron.

The resulting event sample consists of 124 events. It will be referred to as the *inclusive sample* in the following.

Within the inclusive sample the isolation of high-P_T tracks with respect to jets or other tracks in the event is quantified using:

- Their distance D_{jet} to the closest hadron jet in the pseudorapidity-azimuth plane $\eta - \phi$, defined by $D_{jet} = \sqrt{(\eta_{track} - \eta_{jet})^2 + (\phi_{track} - \phi_{jet})^2}$. For this purpose jets are reconstructed using a cone algorithm [10] with $R = 1$ and $E_T^{min} = 5$ GeV. The hadronic nature of a jet is ensured by requiring the fraction of the total jet energy deposited in the electromagnetic calorimeter to be smaller than 0.9 and the jet radius to be larger than 0.1. The jet radius is defined in the $\eta - \phi$ plane as the energy-weighted average distance to the jet axis of all jet components.

- Their distance D_{track} to the closest track in $\eta - \phi$, defined in the same way as D_{jet}. Here all tracks fitted to the interaction vertex with a polar angle greater than $5°$ are considered.

In all of the 124 events at least one hadron jet is found. Figure 1 shows the correlation between D_{track} and D_{jet} for the high-P_T tracks in the inclusive event sample. In most cases the high-P_T tracks are not isolated. This is expected, since the bulk of events are CC interactions with the high-P_T track located within or close to the hadronic shower. However, six high-P_T tracks are found in a region well separated from all other charged tracks and from hadron jets. They belong to six events each with one single isolated high-P_T charged particle.

The nature of the six isolated high-P_T particles is investigated by applying the following lepton identification criteria:

- Electron candidate: A calorimetric energy deposit larger than $5\,\text{GeV}$, with more than 90% of the energy located in the electromagnetic part of the liquid argon calorimeter, has to match geometrically the track.
- Muon candidate: The central track extrapolation must have a total liquid argon energy smaller than 5 GeV in its vicinity, and it has to match geometrically an instrumented iron signal (muon system track or tail catcher energy deposit).

All six isolated high-P_T particles fulfill one of the lepton identification criteria. One is an electron candidate and five are muon candidates.

In summary, after application of an inclusive selection procedure and lepton identification criteria, six events are found with calorimetric missing transverse momentum and an isolated high-P_T lepton candidate, from which five are muon candidates and one is an electron candidate. No event is found with more than one high-P_T lepton candidate. The six events are described in detail in the next section.

2.3 Event Properties

Hereafter the six events with lepton candidates are labelled ELECTRON and MUON-1 to -5. Their event displays are shown in figure 2.

Lepton Signatures

The electron candidate shows an isolated track measured in the central tracker with a specific ionization, $\mathrm{d}E/\mathrm{d}x$, compatible with the passage of a single particle. The track is linked to an energy deposit ($E = 82\,\text{GeV}$, $E_T = 38\,\text{GeV}$) in the electromagnetic part of the calorimeter. The shower pattern is compatible with the expectation for a shower of electromagnetic origin. The measured curvature of the track is compatible with that expected for a negatively charged particle with a transverse momentum of $P_T = 38\,\text{GeV}$. The assignment of a positive charge is incompatible with the measurement at the level of 5 standard deviations.

In all five muon candidates the isolated track is measured in the central tracker, the calorimeter and the chambers of the instrumented iron system. For all tracks the specific ionization, as measured in the central tracker, is consistent with a single minimum ionizing particle traversing the chambers. The track is assigned a positive charge for MUON-1 and -2, and a negative charge for MUON-3 and -4. For MUON-5 the charge is undetermined. The central track is extrapolated through the calorimeter and the coil to the instrumented iron system, taking into account the effect of the magnetic field and the expected multiple scattering and energy loss in the material along the path. For all events the energy depositions in the calorimeter sampled over a path length of ≈ 7 interaction lengths are compatible in shape and magnitude with those expected for a minimum ionizing particle. In four of the five events the central track is linked successfully to a track reconstructed in the muon chambers. In event MUON-5 the instrumented iron signals line up with the extrapolated central track but are recorded near an edge of acceptance, preventing reconstruction of a track in the muon chambers.

The isolated muon candidates penetrate in total more than 14 interaction lengths in the calorimeter and the instrumented iron. In the momentum range of the muon candidates, the probability that an isolated charged hadron would simulate a muon both in the calorimeter and the instrumented iron is estimated to be $< 3 \cdot 10^{-3}$.

In summary the signals seen in the central tracker, the calorimeter and the instrumented iron system support the interpretation of the electron candidate and the 5 muon candidates as e^- and $\mu^\pm$, respectively.

Event Kinematics

In all events a shower with hadronic signature is recorded in the calorimeter. In event MUON-5 no charged particles are found to be correlated with the core of the high-P_T hadronic jet. Event MUON-3 shows in addition to the high-P_T muon a low-P_T positron measured in the central tracker and the calorimeter. No signals are seen in the backward calorimeter, the positron or the photon taggers, apart from an energy deposition of 3 GeV registered for event MUON-4 at the edge of the acceptance in the innermost region of the backward calorimeter.

The event kinematics are quantified using the following variables:

- $\vec{P}_T^{\ell}$: Transverse momentum of the isolated lepton. It is calculated using the calorimetric information for electrons and the central tracker information for muons.
- $\vec{P}_T^X$: Transverse momentum of the hadron system. $\vec{P}_T^X$ is defined as the transverse component of the vector sum of all energy deposits recorded in the liquid argon calorimeter and the tail catcher, except for those associated with isolated leptons (for MUON-3 both the isolated muon and positron are excluded from the system X).
- $P_{||}^X$: Component of $\vec{P}_T^X$ parallel to the transverse direction of the isolated high-P_T lepton.
- $P_{\perp}^X$: Component of $\vec{P}_T^X$ perpendicular to the transverse direction of the isolated high-P_T lepton (the sign of $P_{\perp}^X$ is defined along a y-axis such that $\vec{P}_T^{\ell}$, y, z form a right handed coordinate system).
- P_z^X : Longitudinal momentum of the hadron system.
- E^X : Energy of the hadron system.
- $\vec{P}_T^{miss}$: Missing total transverse momentum of the event. $\vec{P}_T^{miss} = -(\vec{P}_T^{lepton(s)} + \vec{P}_T^X)$ is defined from the vector sum of transverse momenta of all observed final states particles. The quantity P_T^{miss} is identical to P_T^{calo} unless the event contains isolated muons in the final state. Note that in the latter case the P_T^{calo} criterion in the inclusive selection does not automatically imply an imbalance in the total transverse momentum of the event.
- δ : event balance in longitudinal momentum as defined in section 2.2.
- $M_T^{\ell\nu} = \sqrt{(P_T^{miss} + P_T^{\ell})^2 - (\vec{P}_T^{miss} + \vec{P}_T^{\ell})^2}$: high-P_T lepton-neutrino transverse mass, where the measured missing transverse momentum $\vec{P}_T^{miss}$ is attributed to a hypothetical neutrino.

The determination of the global event variables P_T^{miss}, δ and $M_T^{\ell\nu}$ relies on the measurement of the lepton and hadron kinematic variables. In all events the dead material and energy-weighting correction factors applied to the hadron system X in the reconstruction were checked to be compatible with the average corrections to NC hadron jets in the same P_T^X and polar angle domain. For the muon events the measurement of the high-P_T muon track by the central tracker was checked using a sample of NC events, selected such that the positron traverses the same region of the chambers as the muons. In this sample the comparison of the positron track parameters with the calorimetric measurement shows no significant bias of the tracker response, and no smearing towards unphysically high transverse momentum values. In the domain under consideration the resolution of the track momentum is measured to be $\sigma_{P_T}/P_T^2 = 7 \times 10^{-3}$ GeV^{-1}, which is in the same range as the errors quoted for the muon tracks.

The kinematic parameters of the events are summarized in table 1.

For all events an imbalance in total transverse momentum, P_T^{miss}, is observed. This imbalance is ascribed to unobserved particles carrying away transverse momentum. Apart from the events MUON-4

	ELECTRON	**MUON-1**	**MUON-2**	**MUON-3 *)**	**MUON-4**	**MUON-5**
The isolated high-P_T lepton						
Charge	Neg.(5σ)	Pos.(4σ)	Pos.(4σ)	Neg.(4σ)	Neg.(2σ)	unmeasured
P_T^l	$37.6^{+1.3}_{-1.3}$	$23.4^{+7.5}_{-5.5}$	$28.0^{+8.7}_{-5.4}$	$38.6^{+12.0}_{-7.4}$	$81.5^{+75.2}_{-26.4}$	> 44
θ^l	27.3 ± 0.2	46.2 ± 0.1	28.9 ± 0.1	35.5 ± 0.1	28.5 ± 0.1	31.0 ± 0.1
The hadronic system						
P_T^X	8.0 ± 0.8	42.2 ± 3.8	67.4 ± 5.4	27.4 ± 2.7	59.3 ± 5.9	30.0 ± 3.0
$P_{\parallel}^X$	-7.2 ± 0.8	-42.1 ± 3.8	-61.9 ± 4.9	-12.5 ± 2.1	-57.0 ± 5.5	-28.6 ± 3.1
$P_{\perp}^X$	-3.4 ± 0.9	-2.7 ± 1.8	26.8 ± 2.7	-24.3 ± 2.5	-16.3 ± 3.2	-9.1 ± 2.3
P_z^X	79.9 ± 4.4	153.1 ± 9.1	247.0 ± 18.9	183.7 ± 13.6	118.9 ± 12.1	145.4 ± 8.2
E^X	81.1 ± 4.5	162.0 ± 10.0	256.9 ± 19.5	186.8 ± 14.0	141.7 ± 13.7	154.8 ± 9.1
Global properties						
P_T^{miss}	30.6 ± 1.5	$18.9^{+6.6}_{-8.3}$	$43.2^{+6.1}_{-7.7}$	$42.1^{+10.1}_{-5.9}$	$29.4^{+71.8}_{-13.9}$	> 18
δ	10.4 ± 0.7	$18.9^{+3.9}_{-3.2}$	$17.1^{+2.5}_{-1.7}$	$26.9^{+4.2}_{-2.9}$	$43.5^{+19.3}_{-7.2}$	> 22
$M_T^{l\nu}$	67.7 ± 2.7	$3.0^{+1.5}_{-0.9}$	$22.8^{+6.7}_{-4.2}$	$75.8^{+23.0}_{-14.0}$	94^{+157}_{-54}	> 54
*) Positron in MUON-3 : $P_T^e = 6.7 \pm 0.4$, $P_{\parallel}^e = 6.1 \pm 0.4$, $P_{\perp}^e = -2.8 \pm 0.2$, $P_z^e = -3.7 \pm 0.2$						

Table 1: Reconstructed event kinematics (see text). Energies, momenta and masses are given in GeV and angles in degrees. For the charge of the high-P_T lepton the significance of the determination is given. In case of event MUON-5 2σ limits are quoted for the muon momentum and derived quantities.

and MUON-5, a significant deficit is also seen in the longitudinal momentum balance quantified by δ. For the events MUON-4 and MUON-5, the muon momenta are high and only measured with moderate precision resulting in large errors for P_T^{miss} and δ. Additional evidence for undetected particles carrying transverse momentum is provided by the acoplanarity observed in most events (table 1) between the high-P_T lepton and the hadronic system X, quantified by $\Delta\phi = \arctan(P_\perp^X / P_{||}^X)$.

An imbalance in transverse momentum may be faked as a result of measurement uncertainties or high energy proton remnants lost in the beam pipe. In order to assess the significance of the observed imbalance in transverse momentum, we compare in figure 3 the correlation between $\Delta\phi$ and P_T^{miss} for the six events under discussion with that measured in NC events, which are expected to be intrinsically coplanar and balanced in P_T. In order to cover a similar kinematic region, NC events are selected with $10° < \theta^e < 50°$, and, either $P_T^e > 20$ GeV and $P_T^X > 5$ GeV for comparison with the ELECTRON event, or $P_T^e > 10$ GeV and $P_T^X > 25$ GeV for comparison with the MUON events. In the latter case P_T^{miss} is computed using the positron track parameters instead of using the calorimetric information. When compared to the NC events, all candidates except MUON-1 have both high $\Delta\phi$ and high P_T^{miss}. The probability for a NC event to have both $\Delta\phi$ and P_T^{miss} values greater than those measured in a given candidate is determined from a high statistics simulation to 1% for MUON-1 and less than 0.1% for the other candidates.

3 Discussion

In the following we discuss processes within the SM which may yield events with missing transverse momentum and with an isolated high-P_T lepton. The rates predicted for these processes are summarized in table 2.

Predictions for all processes considered are obtained by applying the selection procedure of section 2.2, by requiring a high-P_T lepton with $D_{track} > 0.5$ and $D_{jet} > 1$, and by taking into account trigger efficiencies. Additional isolated leptons, if any, are identified using the same criteria as for the high-P_T lepton but lowering the minimum P_T to 1 GeV. The SM rates quoted do not include events with more than one isolated lepton of the same generation (lepton pair production) since this topology does not correspond to the topologies of the observed six events.

The Monte-Carlo simulations used for the predictions include a full simulation of the H1 detector response.

3.1 Standard Model Processes

- W Production: At parton level a lepton-neutrino pair can be produced via the reactions $e^+q \to e^+q'\ell\nu$ and $e^+q \to \overline{\nu}q'\ell\nu$. The reaction $e^+q \to e^+q'\ell\nu$ dominates by a factor 20. Its Feynman graphs are shown in figure 4a - g. The main diagrams are those involving production of a W ($e^+q \to e^+W^\pm q'$) with subsequent leptonic decay $W^\pm \to \ell^\pm\nu$ (figure 4a-e). An additional source of W production is due to resolved photon interactions. Here the W is produced by fusion of a quark from the proton with a quark from a long-lived hadronic fluctuation of a photon emitted by the incident positron.

  Positively and negatively charged W bosons contribute with similar rates. The expected total cross section is about 60 fb per charge state and leptonic decay channel [11]. The cross section rises towards low values of the transverse momentum P_T^X of the recoil hadron system X, and shows the Jacobian peak around the W mass in the spectrum of the lepton-neutrino transverse mass $M_T^{\ell\nu}$. The resolved photon contribution dominates at very low P_T^X. The cascade decay $W \to \tau\nu, \tau \to \mathrm{e}, \mu$ contributes $\sim 15\%$ of the total accepted rates in the e and μ channels. The scattered positron is expected to be observed in the calorimeters ($\theta < 178\,°$) in 25% of the events.

W production is studied quantitatively with the Monte-Carlo program EPVEC [11], which includes all leading-order parton level diagrams for the reactions $e^+q \to e^+q'\ell\nu$ and $e^+q \to \overline{\nu}q'\ell\nu$ together with the resolved photon contribution. EPVEC is interfaced to the JETSET hadronization program [12]. The cross sections for the leading-order diagrams were checked independently [13].

For the electron channel the acceptance of the selection procedure is 33%. For the muon channel it is only 10%, since here the cut in P_T^{calo} acts as a P_T^X cut.

The rate estimates quoted in table 2 include the following systematic effects:

- the uncertainty in the proton structure function and the QCD scale at which it should be evaluated (a variation from 100 GeV^2 to 10000 GeV^2 was assumed).
- the uncertainty in the photon structure function entering the resolved photon contribution. Since this contribution favours low values of P_T^X only the prediction in the electron channel is affected.
- the uncertainty in the contribution from higher order QCD terms. This was estimated from the effect of including parton showers [14] prior to hadronization.

It should be emphasized that it is presently not known whether an exact computation of higher order QCD terms may change the prediction significantly.

- Z production ($ep \to eZX, Z \to \ell^+\ell^-$): This process will only contribute significantly for the τ - channel and only in case that one τ decays leptonically and the other hadronically. The hadronic final states measured in the six events do not show characteristics of hadronic τ decays. In particular the observed charged particle multiplicities exceed those corresponding to the dominant τ decays (1 or 3 charged particles). The generator EPVEC [11] was used to estimate the expected rate from this channel.

- CC - DIS processes: These events are intrinsically unbalanced in transverse momentum due to the final state neutrino. An isolated lepton can only be produced due to fluctuations in the hadronic final state. The generator DJANGO [15] is used to simulate this contribution.

- NC - DIS processes: These events have intrinsically an isolated positron, but a significant P_T^{calo} can only be produced by fluctuations in the shower development and the detector response. The rate of these events is suppressed by the selection criteria on $\Delta\phi$ and δ (see 2.2). The generator DJANGO [15] is used to simulate this contribution.

- Photoproduction processes: In this class, events with two jets of high transverse momenta could contribute if one jet is observed in the detector and the other jet fluctuates into a single isolated hadron which is identified as a lepton. Contributions are only expected in the muon channel since in the electron channel no significant P_T^{calo} is produced. A muon signature can be generated by a hadron when it either decays in flight into a muon or traverses the detector without hadronic interaction. The expected rate resulting from such a process has been derived from the measured rate of events showing a jet of high transverse momentum ($P_T^{jet} > 25\,\mathrm{GeV}$) recoiling against a single isolated hadron track of $P_T > 10\,\mathrm{GeV}$. Folding this rate with the probability that a hadron is misidentified as a muon (see section 2.3) provides the contribution to our sample.

  A special class of photoproduction processes is the production of a heavy quark pair. In particular bottom quarks may produce via semileptonic decays isolated leptons and (due to the escaping neutrino) a transverse momentum imbalance. The corresponding contribution is estimated using the generator AROMA [16]. Since preliminary measurements of H1 [17] indicate that the cross section for bottom production is too low in AROMA, we use for the rate estimate a fivefold increased cross section.

- Photon-photon interactions ($\gamma\gamma \to \ell^+\ell^-$): Here we consider the interaction of a photon radiated from the positron with a photon radiated from the proton. For these processes one has to differentiate between e^+e^-, $\mu^+\mu^-$, $\tau^+\tau^-$ production in either elastic (no visible hadron recoil) or inelastic processes.

Since the production of e^+e^- does not lead to significant P_T^{calo} this process does not contribute.

The production of $\mu^+\mu^-$ contributes only when one muon of the pair remains undetected. The process contributes in two ways. Firstly, it can contribute to the e channel of our selection via elastic production. In this case the scattered e^+ is registered in the detector and causes the P_T^{calo}. The rate of these events is significantly suppressed by the selection cut on δ (see 2.2). Secondly, this process can contribute to the μ channel in our selection via inelastic production. Here the final state hadrons cause the P_T^{calo}. In both cases the events are expected to have only small P_T^{miss}. The muon which escapes detection in the beam pipe is emitted preferentially in the backward direction and thus it cannot carry a significant transverse momentum.

A small contribution to both electron and muon channels is due to elastic $\tau^+\tau^-$ production with one τ decaying hadronically and the other one leptonically. Due to the small τ mass the decay particles are essentially collinear and the events are thus expected to have small values of $P_\perp^X$. In addition, as already mentioned for the Z contribution, the characteristics of the hadronic final state of the six events are inconsistent with this process.

The photon-photon processes are simulated with the LPAIR [18] generator. A test of this generator has been performed by analysing e^+e^- pair production. In this test, events are selected requiring at least two visible isolated electrons of opposite charge with P_T greater than 10 GeV and 5 GeV respectively. The NC and QED Compton background processes are reduced to a negligible level by demanding in addition either that a third electron be visible in the detector, or that the highest P_T electron be of negative charge and that $\delta < 45$ GeV. In the high P_T range under consideration 17 (quasi-)elastic events ($P_T^X < 2$ GeV) and 8 inelastic events ($P_T^X > 2$ GeV) are observed, compared to expectations of 16.9 and 3.5 respectively. In both elastic and inelastic channels the measured kinematic distributions are compatible with the predictions. With the limited statistics of the test sample in mind, the errors quoted in table 2 for the contribution of the photon-photon process conservatively allow the inelastic contribution to vary within a factor 2.

- Drell-Yan pairs from resolved photon-proton interactions ($q\bar{q} \rightarrow \ell^+\ell^-$): Drell-Yan pairs have intrinsically low transverse momenta and thus cannot accommodate a hadronic system at high P_T^X. Therefore only $\tau^+\tau^-$ pairs could contribute, when one τ decays leptonically and the other hadronically. In order to fullfil the P_T^{calo} cut the $\tau^+\tau^-$ pair must have an invariant mass higher than 50 GeV. In this mass range the cross section extrapolated from fixed target measurements [19] is less than 0.1 fb, resulting in a negligible contribution.

- Halo muon from the proton beam: The proton beam in HERA is accompanied by a flux of halo muons generated by proton losses around the ring. The kinematics of the scattering of such a halo muon on a residual gas nucleon restricts the transverse momenta and δ to be below the values observed in the six events.

Table 2 indicates that W production constitutes the largest contribution followed by the NC process (for e^+ events) and the photon-photon process (for $\mu^\pm$ events). All other processes considered contribute negligibly.

3.2 Comparison of event properties to SM expectation

The one e^- event found is compatible in rate with the expectation from W production, while other processes contribute negligibly. In the μ channel the 5 events found have to be compared with an expectation of 0.8 ± 0.2 events, in which W production and photon-photon processes dominate.

	Electron Channel	Muon Channel
Data	$0\,e^+, 1\,e^-$	5
W production	1.65 ± 0.47	0.53 ± 0.11
Z production	0.01 ± 0.01	0.01 ± 0.01
CC - DIS	0.02 ± 0.01	0.01 ± 0.01
NC - DIS	$0.51 \pm 0.10\,e^+$, $0.02 \pm 0.01\,e^-$	0.09 ± 0.06
Photoproduction	< 0.02	< 0.02
Heavy Quarks	< 0.04	< 0.04
Photon-Photon	$0.09 \pm 0.03\,e^+$, $0.04 \pm 0.01\,e^-$	$0.14^{+0.14}_{-0.07}$

Table 2: Observed and predicted event rates. The limits given correspond to 95% confidence level. Unless stated otherwise the quoted numbers refer to the summed production of both lepton charged states.

The measured kinematic parameters P_T^X and $M_T^{\ell\nu}$ of the six events are compared in figure 5 with the distributions in these variables predicted for W production and photon-photon processes. As already discussed W events accumulate at $M_T^{\ell\nu}$ values close to the W mass and at low or intermediate P_T^X values, whereas photon-photon events concentrate at both low P_T^X and low $M_T^{\ell\nu}$ due to the intrinsic transverse momentum balance of this process.

In the ELECTRON and the MUON-3 events the hadronic recoil systems have relatively small transverse momenta P_T^X and the $M_T^{\ell\nu}$ values show up in the Jacobian peak close to the W mass. If in the MUON-3 event the observed positron is identified with the scattered positron the invariant mass of the muon-neutrino system can be calculated. The result is $M_{\mu\nu} = 82^{+19}_{-12}$ GeV in agreement with the W mass. Both these events show kinematic properties typical for W events.

Event MUON-5 also lies at moderate P_T^X and shows a transverse mass $M_T^{\ell\nu}$ which, though measured at a high value, is compatible within 2 standard deviations with the W interpretation.

Figure 5 shows that the other three muon events are found in regions of phase space where the predicted SM rate is low. Events MUON-2 and MUON-4 show large values of P_T^X, and event MUON-1 shows a small value of $M_T^{\ell\nu}$, both of which are unlikely to occur in the W or photon-photon interpretations.

4 Summary

In positron-proton scattering at HERA, events have been selected requiring an imbalance in calorimetric transverse momentum and the presence of a high-P_T charged particle. While the majority of these events have topologies as expected from deep-inelastic charged current interactions, six events show the prominent signature of an isolated high-P_T lepton (0 e^+, 1 e^-, 2 μ^+, 2 μ^- and 1 μ of undetermined charge) together with evidence for undetected particles carrying transverse momentum.

The total yield of events with one isolated high-P_T lepton which is expected from SM processes is 2.4 ± 0.5 in the $e^\pm$ channel and 0.8 ± 0.2 in the $\mu^\pm$ channel. The main contribution is due to W production, estimated in leading order to be 1.7 ± 0.5 and 0.5 ± 0.1 events respectively. The electron event and one of the muon events are found in a region of phase space likely to be populated by W production. Another muon event can, within its large measurement errors, also be accommodated in a W interpretation. The kinematic properties of the remaining three muon events, together with the overall rate excess in the muon channel, disfavour an interpretation of these events within the SM processes considered.

Acknowledgements

We are grateful to the HERA machine group whose outstanding efforts have made this experiment possible. We thank the engineers and technicians for their work in constructing and now maintaining the H1 detector, our funding agencies for financial support, the DESY technical staff for continual assistance, and the DESY directorate for the hospitality which they extend to the non-DESY members of the collaboration. We thank E. Boos for help in calculations of some reaction cross sections.

References

[1] H1 Collaboration, T. Ahmed et al., DESY preprint 94-248 (1994).

[2] H1 Collaboration, S. Aid et al., Z.Phys.C71 (1996) 211.

[3] M.N. Dubinin and H.S. Song, Phys.Rev. D57 (1998) 2927.

[4] T. Kobayashi, S. Kitamura and T. Kon, Phys.Lett. B376 (1996) 227.

[5] H1 Collaboration, I. Abt et al., Nucl. Instr. and Meth. A386 (1997) 310 and 348.

[6] H1 Calorimeter Group, B. Andrieu et al., Nucl. Instr. and Meth. A336 (1993) 460.

[7] H1 Calorimeter Group, B. Andrieu et al., Nucl. Instr. and Meth. A336 (1993) 499 and A350 (1994) 57.

[8] H1 Spacal Group, R.D. Appuhn et al., Nucl. Instr. and Meth. A386 (1997) 397.

[9] H1 Collaboration, Z.Phys. C67 (1995) 565 and Phys.Lett. B379 (1996) 319.

[10] M.H. Seymour, Z.Phys. C62 (1994) 127.

[11] U. Baur, J.A.M. Vermaseren, D. Zeppenfeld, Nucl. Phys. B375 (1992) 3.

[12] T. Sjöstrand, Comp. Phys. Com. 39 (1986) 347.

[13] E. Boos, private communication.

[14] T. Sjöstrand, Comp. Phys. Com. 82 (1994) 74.

[15] DJANGO 6.2; G.A. Schuler and H. Spiesberger, Proc. of the Workshop Physics at HERA, W. Buchmüller and G. Ingelman (Editors), (October 1991, DESY-Hamburg) Vol. 3 p. 1419.

[16] G. Ingelman, J. Rathsman and G.A. Schuler, Comp. Phys. Comm 101 (1997) 135.

[17] U. Langenegger, Contribution to 33^{rd} Rencontres de Moriond : QCD and High Energy Hadronic Interactions, Les Arcs (1998).

[18] S. Baranov et al., Proc. of Workshop Physics at HERA, W. Buchmüller and G. Ingelman (Editors), (October 1991, DESY-Hamburg) Vol. 3, p. 1478; J.A.M. Vermaseren, Nucl. Phys. B229 (1983) 347.

[19] J. Badier et al., Phys. Lett. 89B (1979) 145.

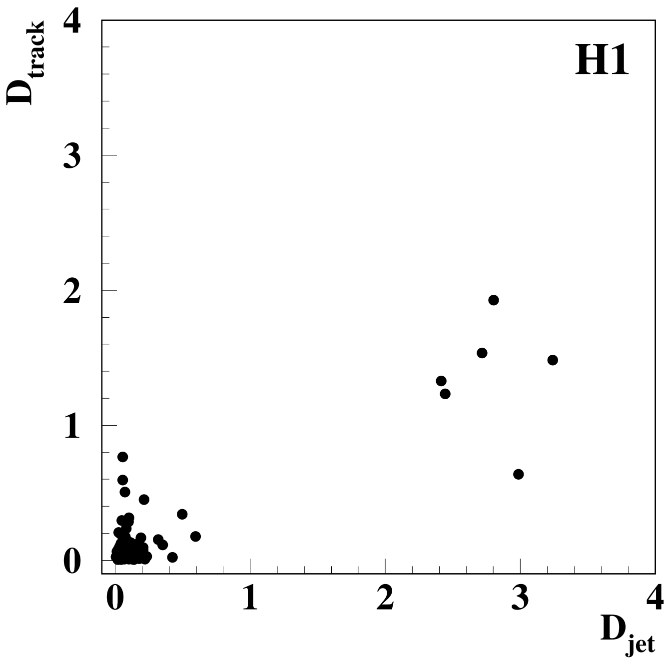

Figure 1: Correlation between the distances D_{jet} and D_{track} (see text) to the closest hadronic jet and track, for all high-P_T tracks in the inclusive event sample.

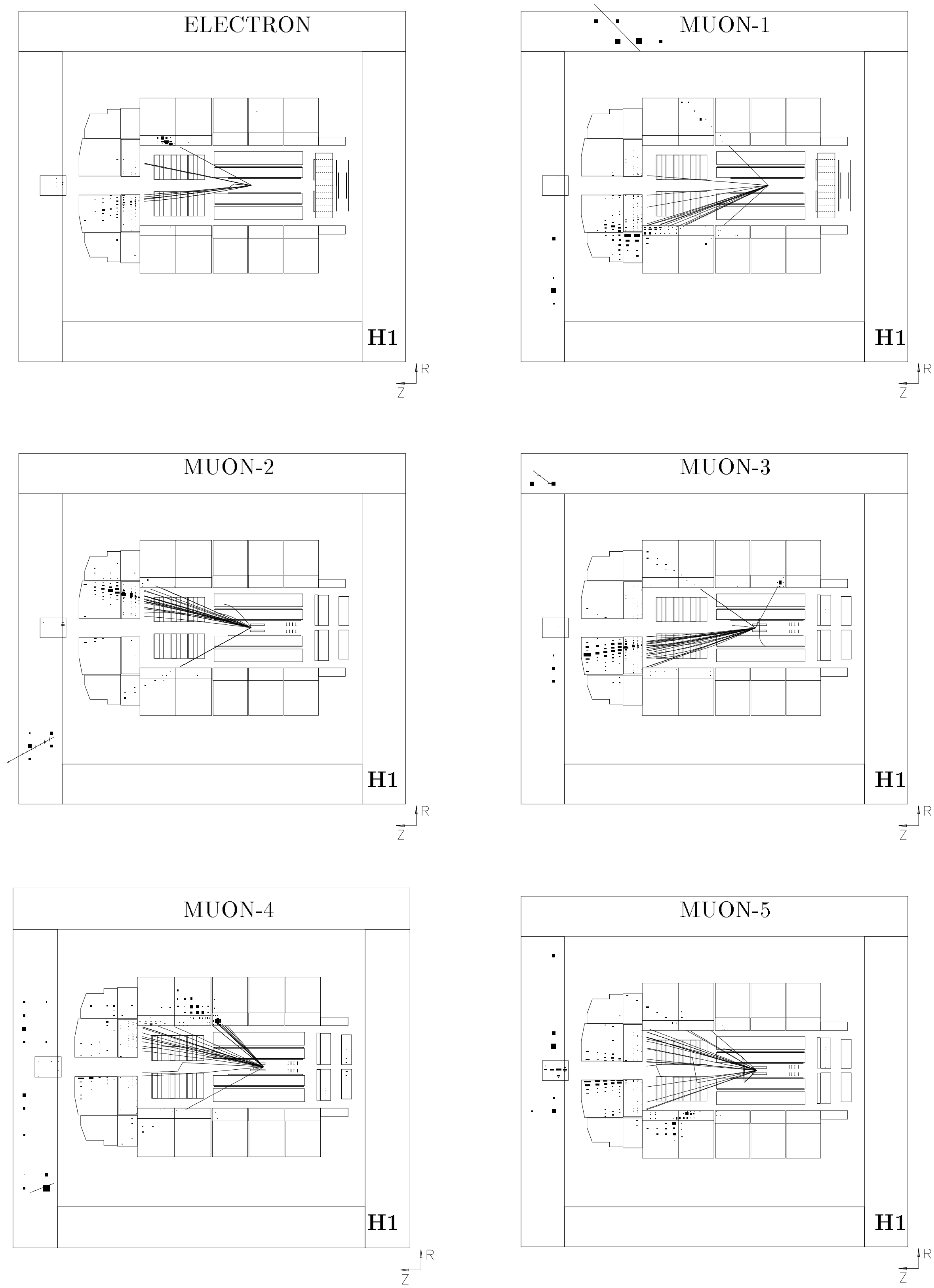

Figure 2: Displays of the six events in the $R - z$ view. Indicated are the reconstructed tracks and the energy depositions in the calorimeters. The HERA positrons and protons enter the detector from the left and right, respectively.

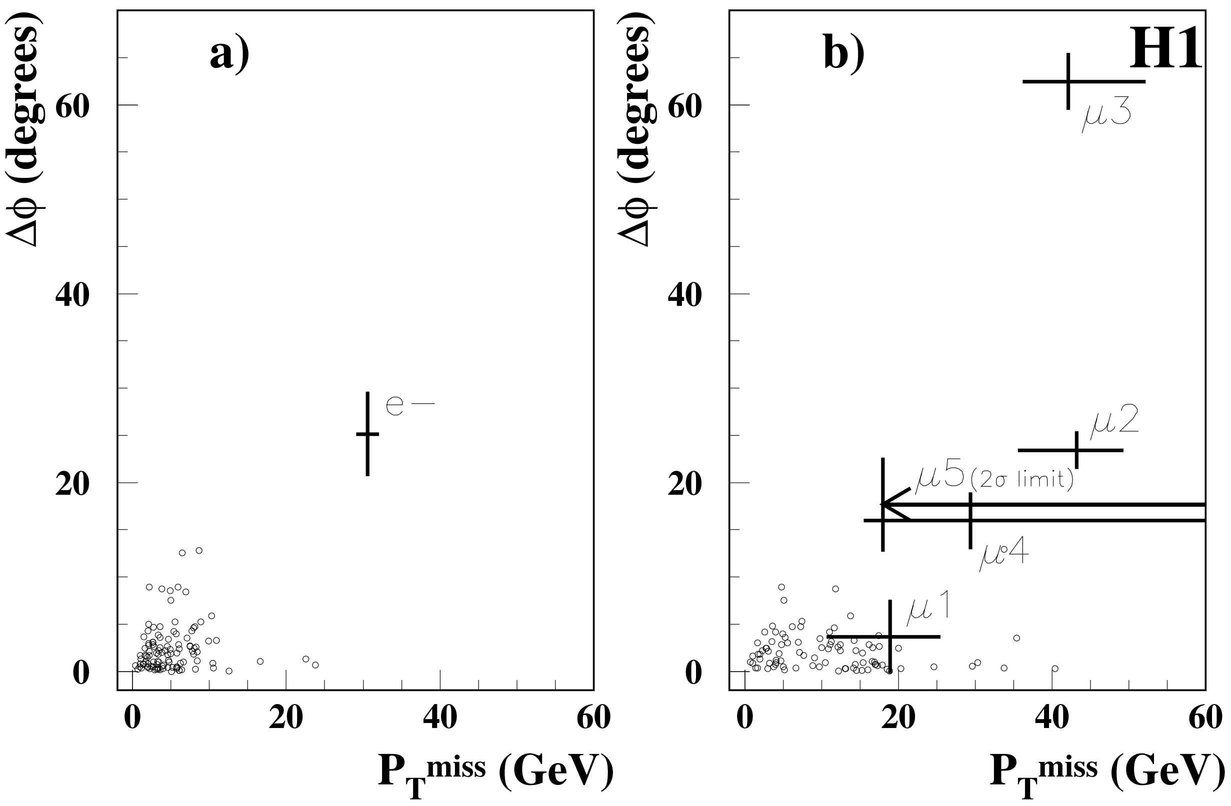

Figure 3: Distribution of events in P_T^{miss} and azimuthal acoplanarity $\Delta\phi$: a) electron channel; b) muon channel. The six events are displayed with their individual measurement errors. For comparison the open circles show the distributions of Neutral Current events (see text), with P_T^{miss} computed in b) from the positron track instead of from the calorimeter shower.

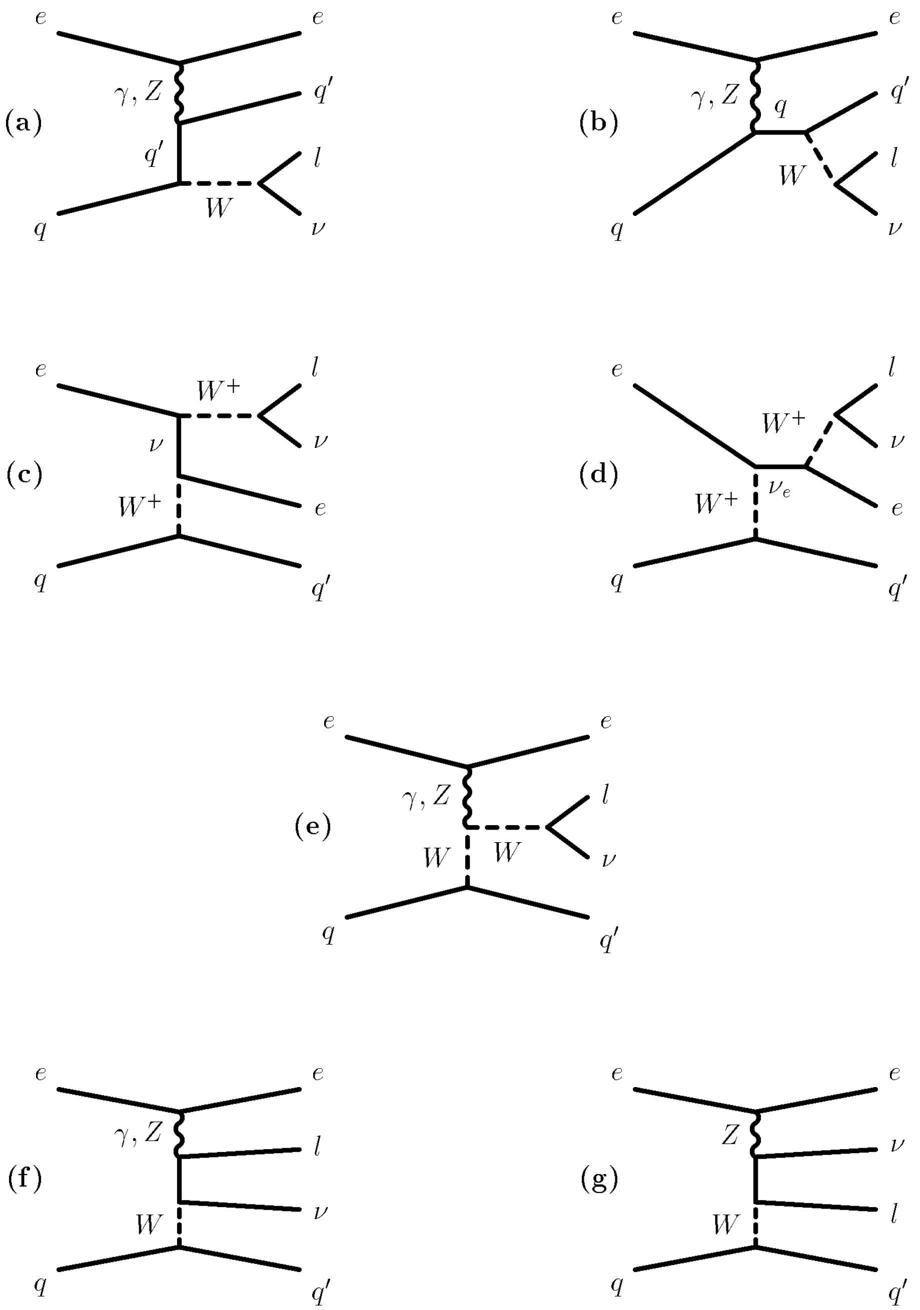

Figure 4: Feynman diagrams for the process $eq \to eq'\ell\nu$

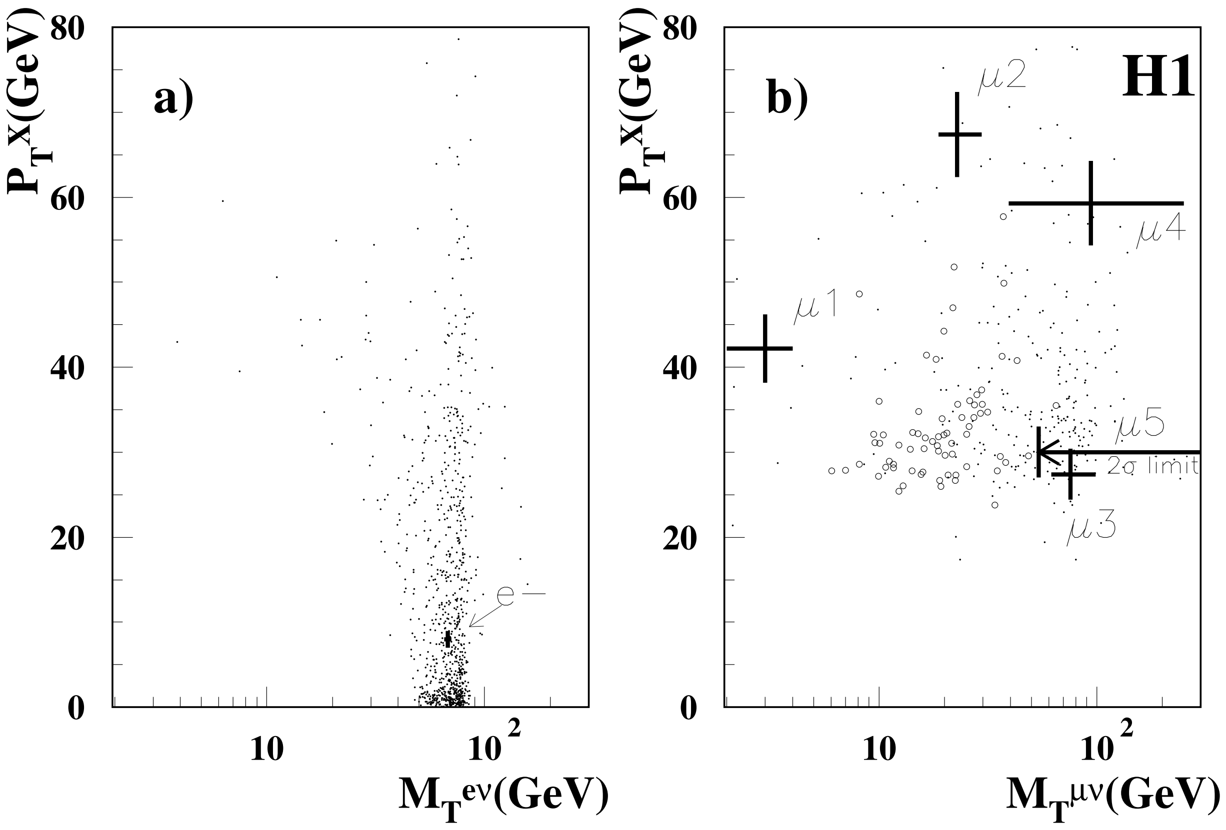

Figure 5: Distribution of events in P_T^X and $M_T^{l\nu}$: a) electron channel; b) muon channel. The crosses indicate the 1-sigma uncertainty on the measured kinematic parameters of the six observed events (for event MUON-5 the 2σ lower limit for $M_T^{l\nu}$ is shown). The dominant SM contributions (dots for W production, open circles for photon-photon processes in the muon channel) are shown for an accumulated luminosity which is a factor 500 higher than in the data. In the muon channel no significant contribution is expected at $P_T^X < 25$ GeV because of the P_T^{calo} cut in the selection procedure.